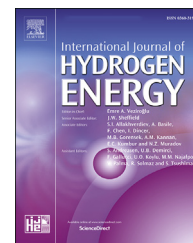




ELSEVIER

Available online at www.sciencedirect.com

ScienceDirect

journal homepage: www.elsevier.com/locate/ijhydene

Determination of the enthalpy of adsorption of hydrogen in activated carbon at room temperature

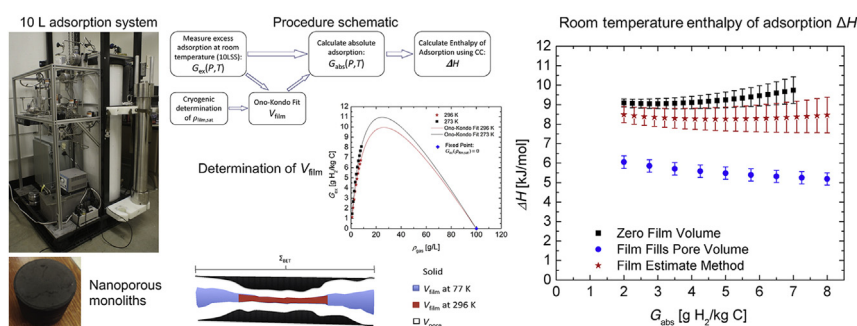
E.W. Knight^{**}, A.K. Gillespie, M.J. Prosniewski, D. Stalla, E. Dohnke, T.A. Rash, P. Pfeifer, C. Wexler^{*}

Department of Physics and Astronomy, University of Missouri, Columbia, MO, 65211, USA

HIGHLIGHTS

- New method to determine the adsorption enthalpy ΔH of hydrogen at room temperature.
- Smaller uncertainty for ΔH than results calculated using common assumptions.
- Estimation of saturation film density, sample and temperature independent.
- Estimation of adsorbed film volume (significantly smaller than pore volume).
- Measurements performed on a large-volume (5.3 L) high-pressure vessel.

GRAPHICAL ABSTRACT



ARTICLE INFO

Article history:

Received 28 September 2019

Received in revised form

13 March 2020

Accepted 4 April 2020

Available online 4 May 2020

Keywords:

Adsorption

Carbon

Hydrogen

Enthalpy of adsorption

Isosteric heat

ABSTRACT

The development of high-performance materials for hydrogen storage by adsorption requires detailed understanding of the adsorbate-adsorbent interactions, e.g., the enthalpy of adsorption ΔH , which measures the interaction strength. The determination of ΔH for a weakly adsorbing gas such as hydrogen in a carbonaceous porous material is difficult experimentally, normally requiring measuring two cryogenic adsorption isotherms. Here we demonstrate a calculation of ΔH based on ca. room temperature adsorption isotherms at 273 K and 296 K using the Clausius-Clapeyron equation. This requires an estimation of the volume of the adsorbed film (~40%, ~12% of the total pore volume at 77 K, 296 K, respectively) obtained from fits of the excess adsorption isotherms to an Ono-Kondo model with the auxiliary use of a fixed point corresponding to the saturation film density (estimated as 100 ± 20 g/L) which appears to be remarkably sample and temperature independent, i.e., a property of the adsorbate. The calculated room temperature enthalpy of adsorption $\Delta H = 8.3 \pm 0.4$ kJ/mol is in excellent agreement with the low-coverage cryogenic

* Corresponding author.

** Corresponding author.

E-mail addresses: ewkth9@mail.missouri.edu (E.W. Knight), wexlerc@missouri.edu (C. Wexler).

<https://doi.org/10.1016/j.ijhydene.2020.04.037>

0360-3199/© 2020 Hydrogen Energy Publications LLC. Published by Elsevier Ltd. All rights reserved.

Room-temperature
Automotive

determination of ΔH . The methodology hereby proposed facilitates reliable calculations of the enthalpy of adsorption at room temperatures for weakly-adsorbing gases.

© 2020 Hydrogen Energy Publications LLC. Published by Elsevier Ltd. All rights reserved.

Introduction

Due to the environmental impact and finite supply of conventional fossil fuels, substantial steps are needed to seek a cleaner, more sustainable fuel source. Hydrogen-based systems only produce water as a byproduct, making it one of the most desirable alternative fuel sources, especially when produced through sustainable and non-polluting methods such as solar electrolysis or biohydrogen [1]. Hydrogen fuel cell systems can be smaller, weigh less, and can be charged in minutes instead of hours compared to batteries [2]. The largest hurdle remains the storage of the gas itself: for hydrogen to be a viable fuel source its low volumetric energy density at ambient conditions (0.0107 MJ/L) must be increased by orders of magnitude to approach the energy density of liquids such as gasoline (31.1 MJ/L) [3]. Current hydrogen-based systems rely solely on liquefying or compressing the gas. Liquefaction requires expensive refrigeration systems to achieve sufficiently low temperatures (~20 K) [4]. Prototype fuel cell vehicles using compression operate at pressures up to 700 bar [4,5]; this level of compression requires large, heavy metallic or expensive carbon fiber gas cylinders that occupy a significant amount of cargo space for storage limiting the passenger/cargo capacity of the vehicle [6,7]. In addition to the practical difficulties of storing hydrogen at such extreme conditions, a significant amount of energy is lost during liquefaction or compression (~1/3 and ~1/5 of the heating value of hydrogen) [8]. Alternatively, systems utilizing adsorption can greatly increase the stored energy density. Adsorbent materials with nanoporous structures utilize the van der Waals attraction between the adsorbent and the hydrogen molecules to create a high density film [9–11] which may be in excess of liquid hydrogen (71 g/L [12]). Various potential adsorbents have been extensively studied, including porous carbons, zeolites, metal-organic-frameworks (MOFs), and porous polymers [13–17].

In order to improve the storage capability of an adsorbent material, research has focused on increasing the surface area, optimizing pore geometry, and increasing the adsorption energy [18]. The hydrogen binding energy for most materials is between 4 and 7 kJ/mol [19–23]. Numerical estimates show that an adsorption energy between 12 and 20 kJ/mol will be necessary for ambient temperature operating conditions [19–24]. One method to increase the adsorption energy in microporous materials is to change the pore width to create overlapping adsorption potentials. For activated carbons, the pore widths can be tuned by adjusting the activation parameters [25,26], and in metal-organic-frameworks (MOFs) the length of the linker can be adjusted to achieve different pore widths [27]. The plausibility of porous carbons for hydrogen storage has motivated a large number of investigations attempting to optimize the storage characteristics [8,10,28–30].

In addition to the adsorbent specific surface area and pore volume, the adsorbate-adsorbant interaction energy or its closely related adsorption enthalpy ΔH are the main quantities that affect the effectiveness of the adsorption process at various temperatures and pressures (the adsorption energy is one of the factors that determines the shape of the adsorption isotherm, particularly in the Henry's law regime) [8–10,13,20,21,23,26,30,31]. A direct measurement of the enthalpy of adsorption ΔH for hydrogen is a relatively difficult process requiring the use of very sensitive microcalorimeters which are not very common. Instead, the more common approach is to measure two adsorption isotherms at close temperatures and ΔH is calculated using the Clausius-Clapeyron (CC) equation [9,32] (the detailed procedure is explained late in the paper). Various factors, however, make this procedure difficult for hydrogen: its weak binding energy make the measurements difficult at room temperature, and measurements at cryogenic temperatures face hurdles related to uncertainties in the determination of cold vs. warm volumes. Additionally, a more fundamental aspect is the fact that the CC equation requires the determination of *absolute* adsorption whereas experimentally only the *excess* adsorption is measured; the conversion between these requires knowledge of the adsorbed film volume which has been not measurable. This has led to assumptions/approximations that result in large uncertainties in the determination of ΔH .

In this study we have constructed a very large volume sample vessel (5.3-L) which is substantially larger than most previously existing hydrogen storage characterization systems. The large sample volume and resulting relatively large amounts of adsorbed hydrogen result in very reliable ca. room temperature excess adsorption isotherms. We then propose a method to determine the adsorbed film volume from Ono-Kondo model fits of the excess adsorption isotherms with the auxiliary use of a fixed point corresponding to the saturation film density which appears to be remarkably sample and temperature independent (a property of the adsorbate). This allows the calculation of *absolute* adsorption isotherms which then are used to obtain the room temperature enthalpy of adsorption ΔH . The method presented here results in significantly lower uncertainties compared to the broad range permitted by the most common assumptions and lacks the unphysical rise with coverage sometimes reported. The results should be applicable to a wide range of samples and temperatures.

Experimental

Adsorbent preparation and characterization

The samples utilized in this work are comprised of monoliths created from a commercially available precursor powdered

activated carbon (PAC): MWV-0260 (MeadWestVaco). The chemical activation was by means of KOH at high temperature [25,31,32]. Carbonaceous adsorbent materials were chosen for this work because they are able to maintain their high storage capacities while withstanding extreme mechanical stress [33]. The precursor PAC was mixed using a rock tumbler with the binder (polyvinylidene chlorid-co-vinyl chloride) (PVDC) in a 0.5:1 binder to PAC ratio. Then 0.5 kg of the mixture was placed inside a cylindrical steel die at 27 °C in 0.1 kg increments where a 760-bar compressive stress was applied after each addition. The monoliths were then heated to 305 °C under stress before being allowed to cool for 16 h while maintaining the mechanical stress. These carbon monoliths were pyrolyzed at 700 °C for 1.5 h under nitrogen prior to measurements. The procedure results in remarkably consistent samples; further detail about the production and characterization of the monoliths can be found in the work by Rash et al. [34] and in U.S patent numbers 8,691,177 [35] and 8,926,932 [36]. For our work, a 2.86 kg batch of monoliths, filling the 5 L sample vessel, was studied (henceforth dubbed BR-0311).

Subcritical nitrogen isotherms on PAC MWV-0260 and small samples of BR-0311 were measured using a Quantachrome Autosorb-1. Results are summarized in Table 1. The Brunauer-Emmett-Teller (BET) [37] surface areas Σ_{BET} were measured using a pressure range of 0.03–0.1 P/P_0 . The cumulative pore volumes V_{pore} were measured at 0.995 P/P_0 by assuming liquid densities within the pores. The pore volume only includes void volume within individual grains and does not include intergranular void space. The skeletal densities ρ_{skel} were measured with helium pycnometry. These ρ_{skel} fall within the typical range of values for amorphous carbon (1.8–2.1 g/cm^3) [25]. The void fraction or porosity is determined by

$$\phi = \frac{V_{\text{pore}}}{V_{\text{pore}} + V_{\text{skel}}} = (1 + (\rho_{\text{skel}} V_{\text{pore}})^{-1})^{-1}. \quad (1)$$

Pore size distributions (PSD) were calculated using quenched solid-state density functional theory (QSDFT) [38–42] assuming slit shaped pores (see Fig. 1). The PSDs for both materials exhibit consistent features. There is an overall reduction from the monolith production process. Some pores were likely clogged with the binder or crushed from the intense mechanical stress. Surface areas and pore volumes can also be reduced from doping the material with other elements such as Boron [43]. The varying pore widths correspond to varying deepness of the potential wells [8,25,44], see Fig. 2: narrower pores where the van der Waals potential of each side of the pore overlap are deep while wider pores have shallower potentials. Numerical simulations involving ensemble averages of different pore sizes weighted by the experimental PSD's [45] are consistent with the idea that narrower pores

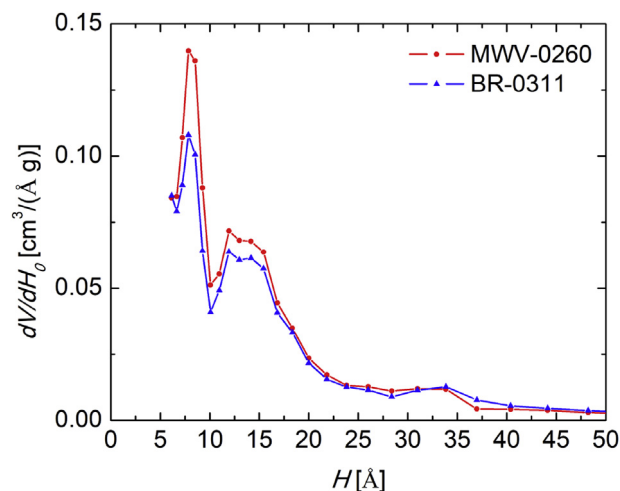


Fig. 1 – Pore size distribution for the PAC precursor, MWV-0260, and the representative monolith, BR-0311, calculated using QSDFT.

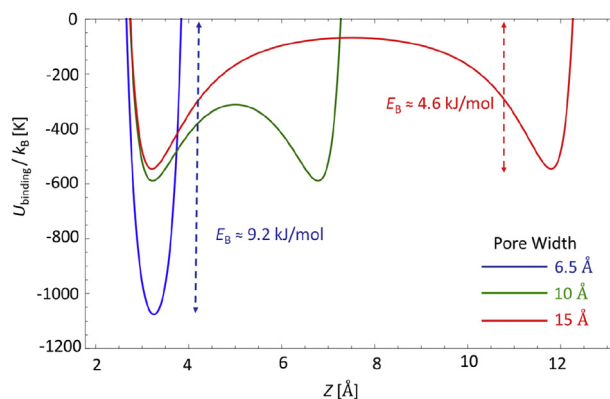


Fig. 2 – Laterally averaged potential energy for hydrogen in slit shaped pores. Binding energy is largest in narrow pores due to the combined adsorption potentials from both sides of the pore [8].

predominantly adsorb the gases at lower coverage while wider pores become more important once the deeper, narrow pores are saturated.

Hydrogen adsorption

Gravimetric excess adsorption measurements were taken on two instruments. A large sample (2.86 kg) was measured with our “10-L Storage System” (10LSS). The 10LSS consists of two 5.3-L modular tanks, filling/discharging mass flow meters, and thermal bath vessels, see Fig. 3. One of the 5.3-L tanks was packed with the 2.86 kg of monoliths. A small sample (~300 mg, 1 cm^3) was measured on a Hiden Isochema HTP1-V.

The gravimetric excess adsorption is the only directly measurable quantity that requires no assumptions about the pore volumes [46], it is calculated from experimental data:

$$G_{\text{ex}}(P) = \frac{m_{\text{H}_2, \text{tank}}}{m_s} - \frac{\rho_{\text{gas}}}{m_s} (V_{\text{tank}} - V_{\text{skel}}), \quad (2)$$

Table 1 – Material properties of precursor PAC and monolith.

Adsorbent	Σ_{BET} (m^2/g)	ϕ	V_{pore} (cm^3/g)	ρ_{skel} (g/cm^3)
MWV-0260	2600	0.76	1.54	2.0
BR-0311	2300	0.74	1.45	2.0

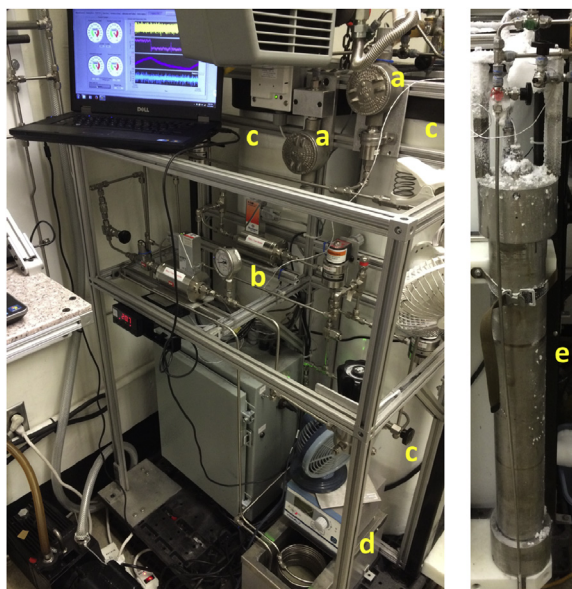


Fig. 3 – 10LSS. Main components are: a) pressure transducers, b) valves and flow meters, c) 2 thermal baths, d) heat exchanger, e) 5.3 L pressure tank with adsorbent BR-0311 inside.

where m_s is the sample mass, $m_{H_2, \text{tank}}$ is the mass of gas in the system, ρ_{gas} is the gas density at the given pressure P , V_{tank} is the volume of the tank or cell, and V_{skel} is the volume of the carbon, (determined with helium pycnometry). In our analysis, in order to mitigate uncertainties [47], we ensured all instruments were well calibrated and leak proof, that samples were outgassed, thermally controlled, and that ultra-purified hydrogen gas (99.999%) was used. The extremely large sample size aided in reducing the relative error of our excess adsorption measurements. G_{ex} measurements are in excellent agreement (overall ~2%) between both aforementioned instruments at two different temperatures, see Fig. 4.

Additional metrics of interest, especially in engineering or applications are the gravimetric and volumetric storage capacities; these are presented for monolithic activated carbon BR-0311 in Appendix A.

Results and discussion

The enthalpy of adsorption ΔH of a gas onto a surface is one of the most important adsorption characteristics; its value along with the specific surface area determine the overall performance of the material for storage or gas separation [31,48,49]. Normally, the determination of ΔH for hydrogen is challenging; a direct determination requiring the use of very sensitive microcalorimeters [50]. Instead, a common approach is to apply the Clausius-Clapeyron equation to two isotherms at two (usually close) temperatures [9,32]:

$$\Delta H = \frac{RT_1 T_2}{T_2 - T_1} \ln \frac{P_2}{P_1}, \quad (3)$$

where T_1 and T_2 are the temperatures at which the two adsorption measurements were taken and P_1 and P_2 are the

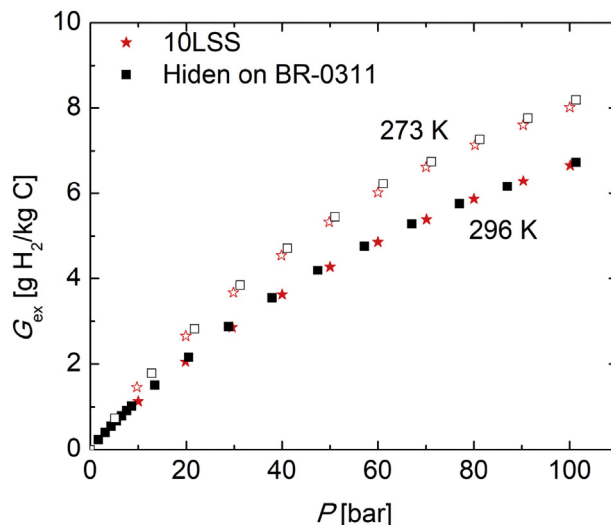


Fig. 4 – Gravimetric excess adsorption isotherms of BR-0311 measured on the 10LSS and Hidden instruments at 273 K (hollow symbols) and 296 K (full symbols).

pressures at which a constant number of particles exist in the adsorbed phase.

As discussed in Refs. [51], the isosteric condition is equal absolute adsorption G_{abs} . Experimentally, only the excess adsorption G_{ex} is measured directly. In addition, cryogenic adsorption isotherms have obvious technical complications (e.g., well-controlled refrigeration/cryostats) and careful calibration (e.g., cold vs. hot volumes) [52]. However, if the volume of the adsorbed film V_{film} were known, it would be possible to calculate the former:

$$G_{\text{abs}} = G_{\text{ex}} + \rho_{\text{gas}} V_{\text{film}}. \quad (4)$$

Unfortunately, V_{film} is not directly observable. Common assumptions utilized in the literature are $V_{\text{film}} = 0$ (i.e., G_{ex} , a significant underestimation) and $V_{\text{film}} = V_{\text{pore}}$ (which generally overestimates G_{abs} since obviously $V_{\text{film}} \leq V_{\text{pore}}$) [53–56]. These assumptions result either overestimation or underestimation of ΔH , respectively [53–56]. Here, we will show how to combine high quality high temperature $G_{\text{ex}}(P, T)$ measurements at ca. room temperature with cryogenic determinations of the adsorbed film density at saturation $\rho_{\text{film, sat}}$ to obtain reasonable estimations of the film volume V_{film} , which enable the determination of the absolute adsorption isotherms $G_{\text{abs}}(P, T)$, and thus the enthalpy of adsorption from the Clausius-Clapeyron equation. The procedure is depicted in Fig. 5 and described in detail in what follows.

Cryogenic determination of adsorbed film densities and volumes

The procedure is to calculate the volume of the adsorbed film from additional experiments. For sufficiently high gas pressures (or ρ_{gas}), when the film density “saturates”, i.e., $\rho_{\text{film}} \approx \rho_{\text{film, sat}}$, $G_{\text{abs}} \approx \text{constant}$, thus using Eq. (6) the volume of the film can be determined:

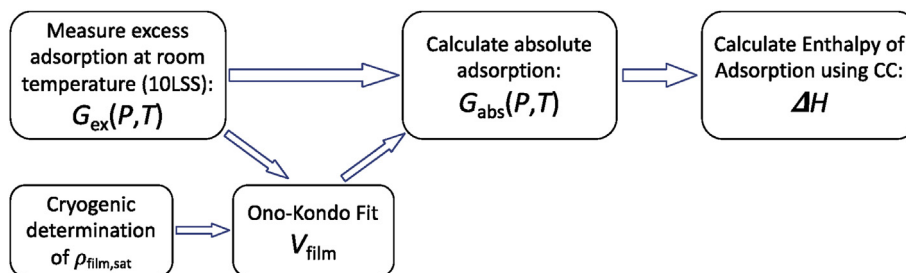


Fig. 5 – Procedure to determine the enthalpy of adsorption from ca. room temperature adsorption isotherms: a) High quality excess adsorption isotherms $G_{ex}(P, T)$ are measured at two close temperatures (10LSS, Figs. 3 and 4) b) Using a low-temperature determination of the adsorbed film density at saturation $\rho_{film,sat}$ (Sec. Cryogenic determination of adsorbed film densities and volume), use the Ono-Kondo equation to determine the adsorbed film volume V_{film} (Eq. (4)). c) Calculate absolute adsorption isotherms $G_{abs}(P, T)$ (Eq. (6)). d) calculate the enthalpy of adsorption ΔH from the Clausius-Clapeyron relation (Eq. (5)).

$$\left. \frac{dG_{ex}}{d\rho_{gas}} \right|_{\rho_{gas} \approx \rho_{film,sat}} = -V_{film}. \quad (5)$$

This high-pressure regime where $\rho_{film} \approx \rho_{film,sat}$ is, however, extremely difficult to reach at room temperature for weakly adsorbing gases such as hydrogen. For example, even at 100 bar the excess adsorption is still growing, and no maximum is even observed (Fig. 4). One possibility is to extrapolate to the high-pressure/high-density regime using the Ono-Kondo model [57,58]:

$$G_{ex} = 2a \frac{\left(1 - \frac{\rho_{gas}}{\rho_{film,sat}}\right) \left(1 - e^{-E_B/RT}\right)}{1 + \left(\frac{\rho_{film,sat}}{\rho_{gas}} - 1\right) e^{-E_B/RT}}, \quad (6)$$

where a is a scaling factor, $\rho_{film,sat}$ is the saturated adsorbed film density, E_B is the binding energy of the gas-solid

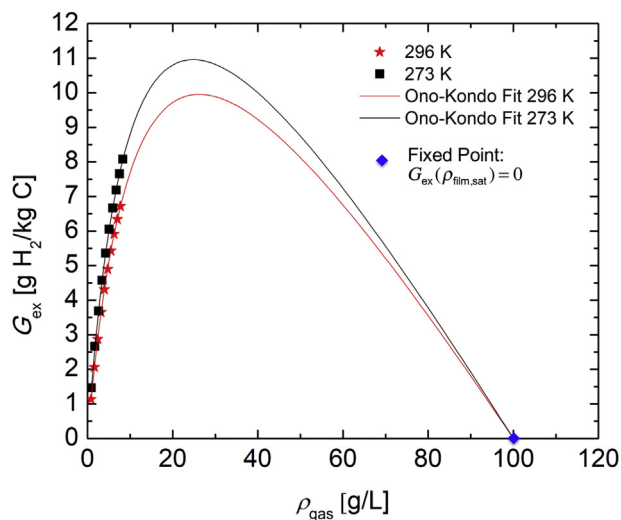


Fig. 6 – G_{ex} isotherms for BR-0311 at 273 K and 296 K up to 100 bar on the 10LSS, with the accompanying Ono-Kondo fits (Eq. (6)) using the fixed point $G_{ex}(\rho_{film,sat}) = 0$, with $\rho_{film,sat} = 100 \text{ g/L}$.

interaction, and R is the ideal gas constant. It seems unlikely that the relatively narrow range of ρ_{gas} accessible at room temperature would yield a trustworthy fit.

However, we have observed that the saturation density $\rho_{film,sat}$ is quite robust across temperatures and different samples. Figs. 7 and 8 show gravimetric excess adsorption isotherms measured using the Hiden HTP1-V instrument in a broad variety of conditions. This instrument, while only capable of using samples $<1 \text{ cm}^3$, can span a broader range of temperatures (77–400 K) and pressures (0–200 bar) than the 10LSS. This capability allows it to reach the high gas density regime, where the adsorbed film becomes saturated and the excess adsorption isotherms exhibit a linear decay with the gas density (Eqs. (5) and (6)). Fig. 7 (a) shows adsorption isotherms for a variety of activated carbons including powders, monoliths and polymer-based materials at 77 K. Donhke et al. [68] have shown that, in this regime, the saturated adsorbed film volume is given by the slope $V_{film} = dG_{ex}/d\rho_{gas}$, and the extrapolation to where the line crosses the abscissa ($G_{ex} = 0$) provides a good estimate for the saturated film density, $\rho_{film,sat}$. It is remarkable that in all samples, the estimation of $\rho_{film,sat}$ (97–107 g/L) is higher than that of liquid H_2 (71 g/L) and is quite independent of the sample specific surface area, see Fig. 7 (b) [66,68,69]. Additionally, the almost linear relation between V_{film} and specific surface area, in Fig. 7 (c), indicate a common film thickness $t_{film} = V_{film}/\Sigma_{BET} \approx 3 \text{ \AA}$ which is significantly lower than the typical pore sizes $> 7 \text{ \AA}$. Across a wide range of temperatures (77–173 K), the estimation of $\rho_{film,sat}$ (100–112 g/L) on BR-0311 is also higher than that of liquid H_2 (71 g/L) and is quite independent of temperature, see Fig. 8 (b) [68,69]. Additionally, V_{film} tends to decrease with increasing temperature, see Fig. 8 (c) which, as an aside, is similar to what was observed with methane as temperatures increase [70].

The fact that $\rho_{film,sat}$ is sample and temperature independent, at least empirically, makes it a property of the adsorbate, i.e., for a given material, a cryogenic temperature determination of $\rho_{film,sat}$ would be valid at almost any other temperature (and likely may even be valid to other materials). The reason for this robustness is that at saturation the film is densely packed so that the dominant effect is the hydrogen to hydrogen repulsion which is very sharp (the interaction

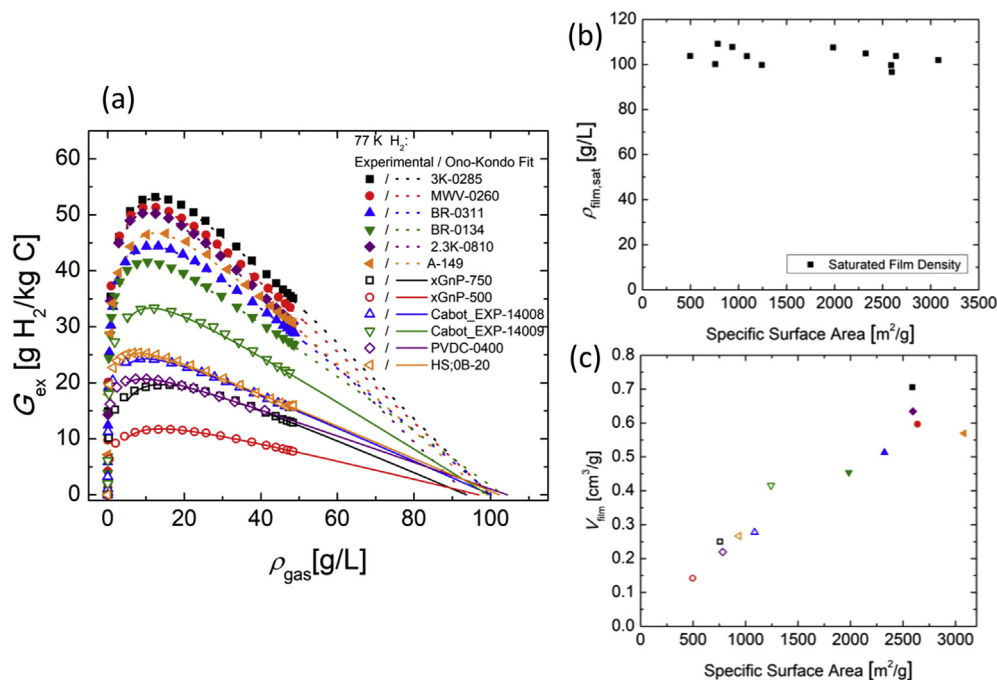


Fig. 7 – (a) G_{ex} vs ρ_{gas} at 77 K measured on the Hiden for a variety of samples. The better performing samples exhibit the linear regime to experimentally determine the V_{film} and $\rho_{film,sat}$. (b) $\rho_{film,sat}$ vs specific surface area, demonstrating no clear dependence. (c) V_{film} , specific surface area demonstrates a linear trend.

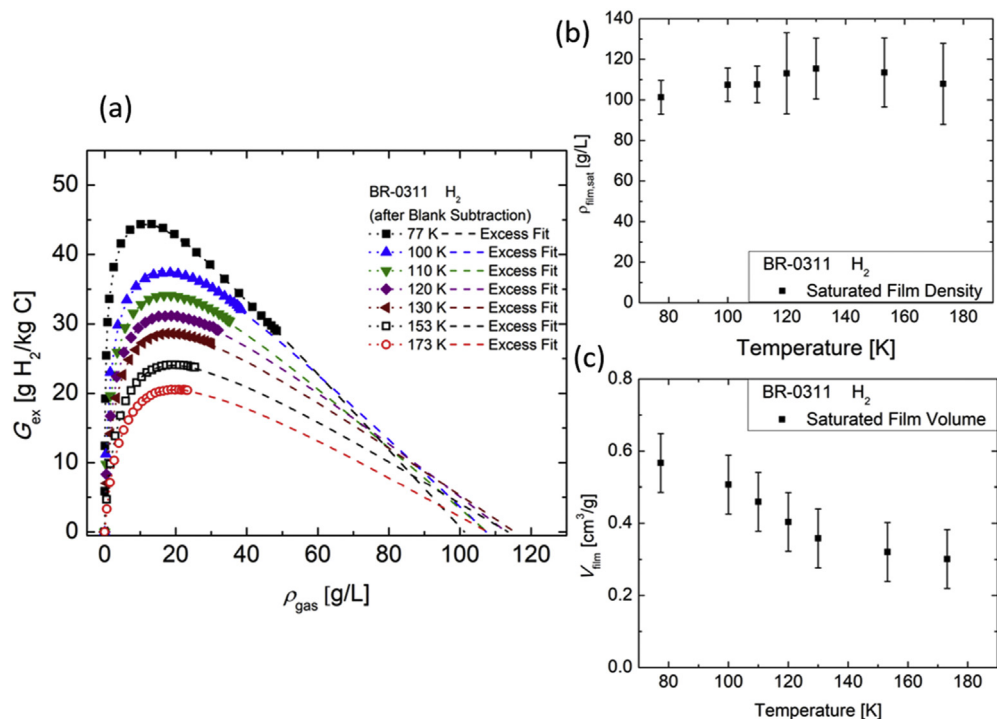


Fig. 8 – (a) G_{ex} vs ρ_{gas} across a 100 K temperature range for BR-0311 measured on the Hiden. The better performing samples exhibit the linear regime to experimentally determine the V_{film} and $\rho_{film,sat}$. (b) $\rho_{film,sat}$ vs temperature remains constant. (c) V_{film} vs temperature demonstrates the decreasing V_{film} with increasing temperature.

potential rises very abruptly at small distances). This determination quite useful for future developments.

Conversely, V_{film} is seen to decrease with increasing temperature. We speculate that the reason for this behavior is that

at higher temperatures, the adsorption occurs only in the deepest binding sites, normally associated with narrower pores (whereas at lower temperatures the adsorbate gas would have access to more binding sites). Fig. 9 illustrates this

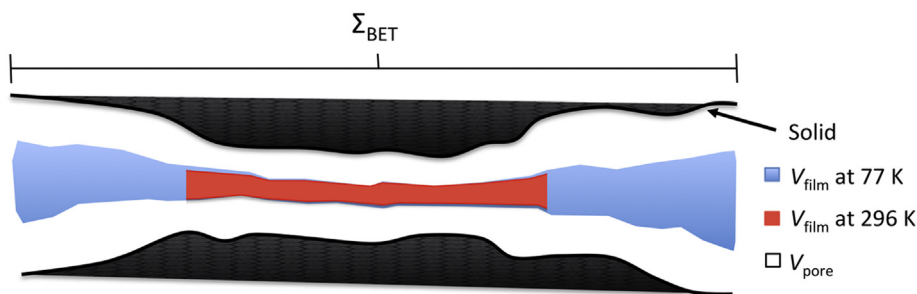


Fig. 9 – Illustration of the decrease of V_{film} with increase of temperature. At lower temperature narrow and wide pores contribute to the adsorption; at higher temperatures only the narrower pores do.

idea: more pore sizes contribute to the overall V_{film} as temperature decreases.

Based on these results, we make the assumption that these values of $\rho_{\text{film,sat}}$ remain valid at higher temperatures, at least as a first order approximation. This adds one important fixed point to the isotherm ($G_{\text{ex}}(\rho_{\text{film,sat}}) = 0$, Fig. 6). Only the slope $dG_{\text{ex}}/d\rho_{\text{gas}}$ at $\rho_{\text{gas}} \approx \rho_{\text{film,sat}}$ is important in what follows. For the calculations that follow, we chose $\rho_{\text{film,sat}} = 100 \pm 20$ g/L (Figs. 7 and 8). The error assumed for $\rho_{\text{film,sat}}$ is estimated from the (i) error estimates of the fitting parameters of the Ono-Kondo model for $G_{\text{ex}}(\rho_{\text{gas}})$ in Figs. 7 and 8, (ii) the dispersion of values of $\rho_{\text{film,sat}}$ for different samples, and (iii) the dispersion of values of $\rho_{\text{film,sat}}$ for sample BR-0311 at different temperatures (neglecting a possible small trend in $\rho_{\text{film,sat}}(T)$). Calculating the slope of the Ono-Kondo fit in the high gas density regime then yields the volume of the adsorbed film V_{film} [59,60].

These assumptions result in a good fit to the data (Table 2) that shows a reasonable extrapolated local maximum and high gas density regime (Fig. 6). With the Ono-Kondo fit described above, V_{film} can be calculated from the slope of the high gas density regime (Eq. (5)).

Interestingly, for BR-0311 the calculated V_{film} (Table 2) are only ~12% of V_{pore} (1.45 cm³/g), at cryogenic temperatures (Fig. 8) $V_{\text{film}} \approx 0.58$ cm³/g (~40% of V_{pore}). The uncertainty in the determination of V_{film} predominantly arises from the conservatively estimated uncertainty range for $\rho_{\text{film,sat}} = 100 \pm 20$ g/L (Figs. 7 and 8).

Using this determination of V_{film} the absolute adsorption isotherms for 273 and 296 K can be calculated (Eq. (4)) and are shown in Fig. 10 (the uncertainty of G_{abs} arises predominantly from that of V_{film} , see Eq. (4)) along with fits to the Modified Redlich-Peterson model (MRP with $R^2 > 0.9999$) [61]:

$$G_{\text{abs}} = \frac{a(bP)^{1-c}}{1 + (bP)^{1-c}} \quad (7)$$

Table 2 – Parameter a and E_B from the Ono-Kondo fits and the calculated adsorbed film volume and ratio to total pore volume at 296 and 273 K for sample BR-311 resulting from $\rho_{\text{film,sat}} = 100 \pm 20$ g/L.

T (K)	A	E_B (kJ/mol)	R^2	V_{film} (cm ³ /g)	$V_{\text{film}}/V_{\text{pore}}$
296	10.5 ± 0.5	5.0 ± 0.6	0.99993	0.17 ± 0.05	0.12
273	10.6 ± 0.5	5.0 ± 0.6	0.99985	0.18 ± 0.05	0.12

These fits are useful to interpolate between experimental points and determine points of constant coverage at the two temperatures in the Clausius-Clapeyron relation (Eq. (3)) [51]. The resulting enthalpy of adsorption $\Delta H(P)$ is shown in Fig. 11; for comparison, a cryogenic temperature determination of ΔH is also shown.

In Fig. 11 (b), three different V_{film} assumptions were used to determine G_{abs} and to calculate the enthalpy of adsorption. For $V_{\text{film}} = 0$ ($G_{\text{abs}} = G_{\text{ex}}$), this leads to a larger enthalpy of adsorption (9 kJ/mol) and an unphysical increase at larger coverage [51] (as discussed, at larger coverage shallower sites should be filled, so for heterogeneous samples ΔH should decrease with coverage). The assumption $V_{\text{film}} = V_{\text{pore}}$ ($G_{\text{abs}} = G_{\text{st}}$, see Appendix A) leads to an enthalpy of adsorption that is significantly smaller (6 kJ/mol). Since these two approximations are the most extreme assumptions regarding the V_{film} , an upper and lower bound are set on the enthalpy of adsorption. This narrows the possible values of the enthalpy of adsorption to a 3 kJ/mol range, a 30–50% error.

Using our V_{film} estimate yields a relatively constant $\Delta H = 8.3 \pm 0.4$ kJ/mol at low coverage, and $\Delta H = 8.3 \pm 0.8$ kJ/mol at high coverage in the 273–296 K range (the error is

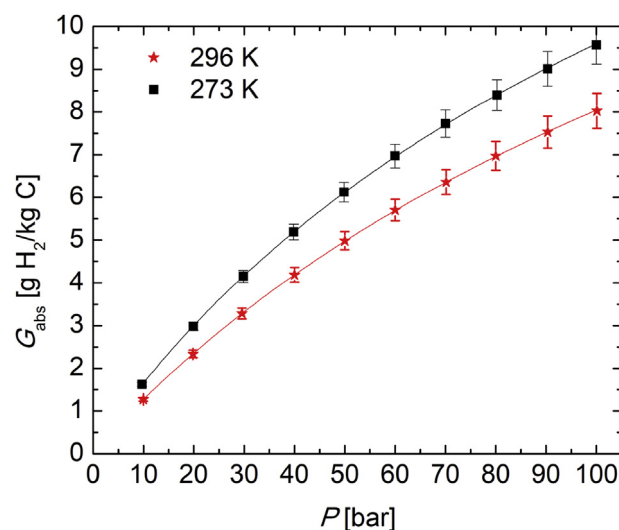


Fig. 10 – Absolute adsorption isotherms $G_{\text{abs}}(P)$ for BR-0311 using the calculated V_{film} (Eq. (5)), with the accompanying Modified Redlich-Peterson fit (Eq. (7)) [61]. Error bars are predominantly due to the uncertainty in V_{film} .

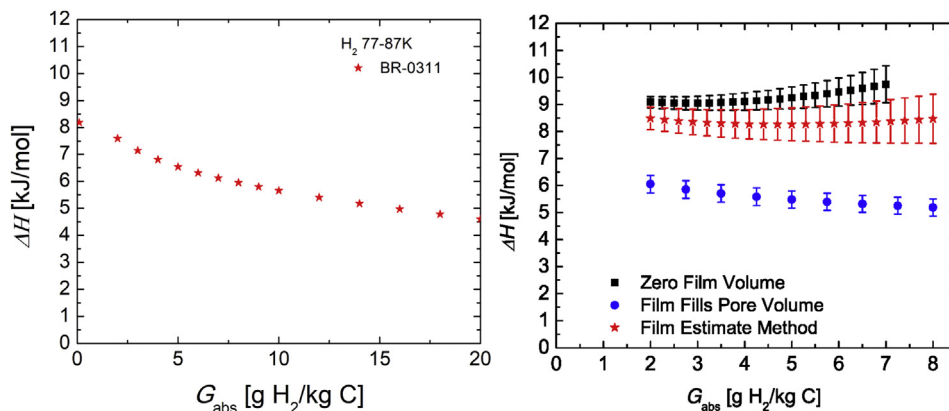


Fig. 11 – (a) Enthalpy of adsorption calculated of BR-0311 using 77 and 87 K isotherms (Eq. (3)). (b) Enthalpy of adsorption using three different film volumes at room temperature (273 and 293 K): (i) the calculated film volumes from the Ono-Kondo fits (red), (ii) the film volume equal to zero $G_{abs} = G_{ex}$ (isoexcess) (black), and (iii) the film volume equal to the pore volume $G_{abs} = G_{st}$ (isostorage, see Appendix A) (blue). (For interpretation of the references to colour in this figure legend, the reader is referred to the Web version of this article.)

dominated by the uncertainties in G_{abs} (Fig. 10)). This is extremely close to the values calculated at 77 and 87 K of 8.2 kJ/mol at low coverage. This demonstrates how the high temperature ΔH corresponds to the low-coverage values at low temperatures. This is because at higher temperature, only the sites with the deepest potentials are populated (these deep potential sites are the ~ 8 kJ/mol wells, at cryogenic temperatures, the high binding energy sites are occupied first at low coverage and then more shallow potential sites down to 5 kJ/mol become occupied). For adsorption onto a substrate without localized binding (i.e., H_2 molecules are free to move in the two dimensions parallel to the adsorbate, as expected at room temperature [8]) we expect $\Delta H = E_B + RT/2 \approx E_B + 1.3$ kJ/mol (see Appendix B). The ΔH hereby calculated has some degree of inconsistency with the binding energy estimates of the Ono-Kondo fit ($E_B = 5.0 \pm 0.6$ kJ/mol, Table 2).

Summary and conclusions

We developed a new methodology for determining the enthalpy of adsorption ΔH for hydrogen on activated carbon at room temperature. The methodology is based on (i) measuring two high-quality ca. room temperature adsorption isotherms, (ii) calculating the absolute adsorption isotherms with the aid of cryogenic estimations of the adsorbed film volume, (iii) using the Clausius-Clapeyron equation to calculate ΔH . We find $\Delta H \approx 8.3$ kJ/mol at room temperature, which agrees within 1.2% of the deepest binding adsorption sites measured at 77–87 K (justified because at room temperature only the deepest binding sites contribute to adsorption). This methodology provides a lower uncertainty determination of ΔH than other methods that either neglect or overestimate the volume of the adsorbed film, and further lacks the unphysical rise with coverage sometimes reported. Additionally, we observed that the saturated film density $\rho_{film,sat} \approx 100$ g/L which is quite robust and appears to be reasonably independent the sample and temperature. Thus the proposed methodology for ΔH may be applied to other adsorbents/adsorbates

without the cost or effort of cryogenic refrigeration or very large pressures (a determination $\rho_{film,sat}$ would be required for other adsorbates).

Acknowledgements

The authors would like to thank Matthew Beckner, Lucyna Firlej, Bogdan Kuchta, Joseph Schaeperkoetter and Jimmy Romanos for useful discussions. We would like to acknowledge MeadWestvaco (currently WestRock) for providing materials for analysis. This work was supported by the United States Department of Defense, Naval Surface Warfare Center under Contract No. N00164-07-P-1306 and N00164-08-C-GS37, the United States Department of Energy, Energy Efficiency and renewable Energy under contract No. DE-FG36-08G018142, the California Energy Commission under contract No. 500-08-022, and the University of Missouri.

Appendix A. Engineering adsorption characteristics of interest

Additional quantities of interest, especially for engineering metrics, are the gravimetric and volumetric storage capacity. They can be calculated from excess adsorption and porosity measurements. Gravimetric storage capacity is defined as the total amount of adsorbate gas stored per mass of adsorbent. It can be calculated as

$$G_{st} = G_{ex} + \frac{\rho_{gas}}{m_s} V_{void} = G_{ex} + \frac{\rho_{gas}}{m_s} \phi V_{system} = G_{ex} + \frac{\rho_{gas}}{\rho_{skel}} (\phi^{-1} - 1)^{-1}, \quad (8)$$

where V_{void} is total void volume of the system which is equal to the total volume available to the adsorbate gas. In the second expression we used $V_{void} = \phi V_{system}$ in order to define gravimetric storage capacity in terms of the porosity (see Table 3). The last expression shows gravimetric storage capacity in terms of the porosity.

Table 3 – Storage metrics for the monolith sample at 296 and 273 K measured on the 10LSS at 100 bar: gravimetric excess, gravimetric storage, volumetric storage, and total mass of H₂ stored.

T (K)	G _{ex} (g/kg)	G _{st} (g/kg)	V _{st} (g/L)	Mass H ₂ stored (g)	V _{st} /ρ _{gas}
296	6.6	17	9.2	49	1.2
273	8.0	19	10.4	55	1.3

The void space between individual grains of adsorbent material needs to be accounted for in a tank system [62]. The packing fraction of a system depends on the amount of intergranular void space present [34,63,64]. The volumetric storage capacity is defined as the total amount of adsorbate gas in the system normalized to the system volume. Since the total mass of gas stored in the system is the same as in the calculation of gravimetric storage capacity, one only needs to multiply by the density of the system to convert to volumetric storage capacity. Therefore, volumetric storage capacity can be calculated by Ref. [65].

$$V_{st} = G_{ex}\rho_{skel}(1 - \phi) + \rho_{gas}\phi. \quad (9)$$

here V_{st} and G_{st} are related through several factors including porosity and excess adsorption. Fig. 12 demonstrates the possible variance in storage capacities for activated carbon samples that have a typical ρ_{skel} ≈ 2.0 g/cm³.

Remarkably, both gravimetric and volumetric storage capacities values measured on the large 3 kg sample in the 10LSS agree within 1% to the values measured on the ~300 mg samples in the Hidden instrument across all pressures, see Fig. 13. This demonstrates that despite the amorphous structure of these carbon samples, they are scalable (by a factor of 10,000) and provide consistent structural and storage performance results [64]. Further detail about the 10LSS can be

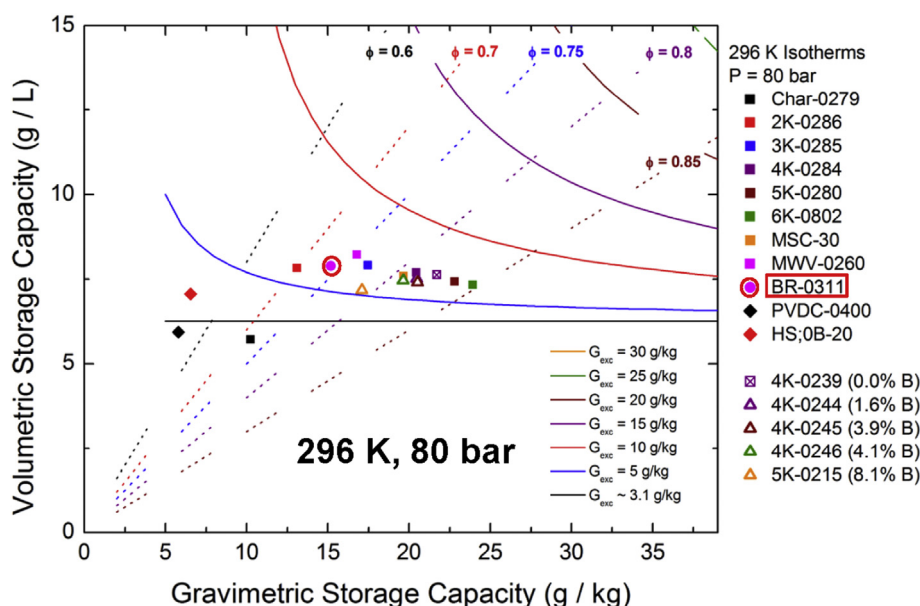


Fig. 12 – Volumetric (V_{st}) vs. gravimetric (G_{st}) storage capacities, with curves of constant excess adsorption (G_{ex}) and constant porosity (φ). Reproduced from Ref. [66]. Our sample BR-0311 is highlighted.

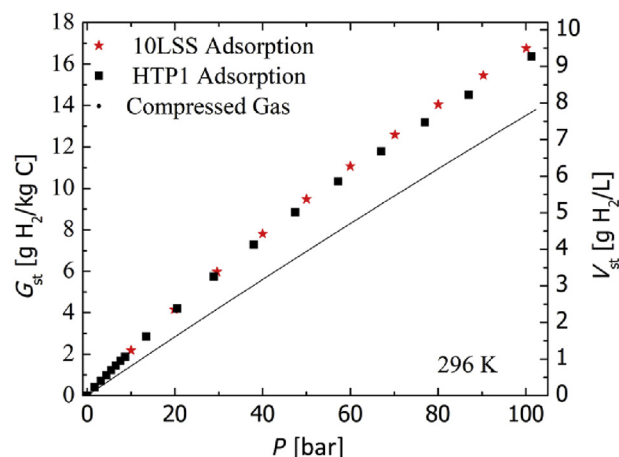


Fig. 13 – Gravimetric (G_{st}) and volumetric (V_{st}) storage capacities measured by the 10LSS and HTP1-V at 296 K.

found in our previous work [66,67] and the work done by Rash et al. [34].

Appendix B. Difference between the enthalpy of adsorption and the adsorption binding energy

Even though they are different, often the enthalpy of adsorption and the adsorption are used interchangeably in the literature, as they are comparable measures of the interaction between the adsorbate and adsorbent. Given the difference between $\Delta H = 8.3 \pm 0.1$ kJ/mol calculated (Sec. Results and discussion) and $E_B = 5.0 \pm 0.6$ kJ/mol estimated in the Ono-Kondo fit (Table 2), it is worth to clarify the possible differences between the two. Let us focus on the enthalpy of the gas phase first (per mol):

$$H_{\text{gas}} = \langle E \rangle + PV = \frac{(3+p)RT}{2} + RT, \quad (10)$$

where $p = 0, 2$ for monoatomic, diatomic molecules, and we have assumed that vibrational degrees of freedom are heavily quantized and the ideal gas law is satisfied. If we assume that the adsorbed volume is much smaller than that for the gas, $H_{\text{ads}} \approx \langle E \rangle$, and consider the adsorption potential as a well of depth U_B where particles are confined by a harmonic potential in $d = 1, 2$, or 3 dimensions with frequencies ν_i (and are free to move in the remainder $3 - d$ dimensions) [8] then

$$H_{\text{ads}} \approx \langle E \rangle = -U_B + RT \sum_{i=1}^d \frac{(h\nu_i/2k_B T)}{\tanh(h\nu_i/2k_B T)} + \frac{(3-d+p)RT}{2}, \quad (11)$$

where h is Planck's constant and the quantization of energy levels of the harmonic oscillators was explicitly considered. We also assume that the rotational degrees of freedom are not significantly affected by the adsorption [71,72]. We thus obtain:

$$\Delta H = H_{\text{gas}} - H_{\text{ads}} = U_B + \frac{(d+2)RT}{2} - RT \sum_{i=1}^d \frac{(h\nu_i/2k_B T)}{\tanh(h\nu_i/2k_B T)}. \quad (12)$$

We now consider the following scenarios (see Ref. [8] for more details).

- a) *Mobile adsorption* (particles are free to move in the xy plane, $d = 1$) in the *classical limit* ($k_B T \gg h\nu$):

$$\Delta H = U_B + \frac{RT}{2}. \quad (13)$$

- b) *Mobile adsorption* (particles are free to move in the xy plane, $d = 1$) in the *quantum limit* ($k_B T \ll h\nu$):

$$\Delta H = \left(U_B - N_A \frac{h\nu_i}{2} \right) + \frac{3RT}{2} = E_B + \frac{3RT}{2}, \quad (14)$$

where in the last term we considered the fact that the true binding energy is shifted by the zero-point energy of the oscillators (N_A normalizes the oscillator energy from per particle to per mol).

- c) *Localized adsorption* (particles are tied to local adsorption sites, $d = 3$) in the *classical limit* ($k_B T \gg h\nu$):

$$\Delta H = U_B - \frac{RT}{2}. \quad (15)$$

- d) *Localized adsorption* (particles are tied to local adsorption sites, $d = 3$) in the *quantum limit* ($k_B T \ll h\nu$):

$$\Delta H = \left(U_B - N_A \frac{3h\nu}{2} \right) + \frac{5RT}{2} = E_B + \frac{5RT}{2}. \quad (16)$$

Identical results may be obtained using the Clausius-Clapeyron equation for ΔH and a Langmuir adsorption model using localized/mobile Henry's law constants as in Ref. [8].

REFERENCES

- [1] Saur G, Milbrandt A. *Renewable hydrogen potential from biogas in the United States*. Golden, CO: National Renewable Energy Laboratory; 2014.
- [2] Saur G, Milbrandt A. *Renewable Hydrogen Potential from Biogas in the United States*. Nat Renewab Energy Lab 2014. <https://doi.org/10.2172/1149657>.
- [3] Thomas G. *Overview of storage development DOE hydrogen program*. Sandia Natl Lab 2000;9.
- [4] Department of Energy Office of Fuel Cell Technologies. *Hydrogen storage*. <https://www.energy.gov/eere/fuelcells/hydrogen-storage>; 2018.
- [5] Field K. *Toyota mirai hydrogen fuel cell vehicle review*. Cleanroom Technol 2018. <https://cleantechnica.com/2018/06/16/toyota-mirai-hydrogen-fuel-cell-vehicle-review-cleantechnica-exclusive> (last accessed by us Sep/2018).
- [6] Eberle U, Müller B, von Helmolt R. *Fuel cell electric vehicles and hydrogen infrastructure: status 2012*. Energy Environ Sci 2012;5:8780–98. <https://doi.org/10.1039/c2ee22596d>.
- [7] Berry GD, Aceves SM. *Onboard storage alternatives for hydrogen vehicles*. Energy Fuels 1998;12:49–55. <https://doi.org/10.1021/ef9700947>.
- [8] Burrell J, Kraus M, Beckner M, Cepel R, Suppes G, Wexler C, et al. *Hydrogen storage in engineered carbon nanopores*. Nanotechnology 2009;20:204026. <https://doi.org/10.1088/0957-4484/20/20/204026>.
- [9] Rouquerol J, Rouquerol F, Sing KSW. *Adsorption by powders and porous solids: principles, methodology and applications*. Academic Press; 1998.
- [10] Pfeifer P, Burrell JW, Wood MB, Lapilli CM, Barker SA, Pobst JS, et al. *High-surface-area biocarbons for reversible on-board storage of natural gas and hydrogen*. MRS Proc 2007;1041. <https://doi.org/10.1557/PROC-1041-R02-02>.
- [11] Golebiowska M, Roth M, Firlej L, Kuchta B, Wexler C. *The reversibility of the adsorption of methane–methyl mercaptan mixtures in nanoporous carbon*. Carbon 2012;50:225–34. <https://doi.org/10.1016/j.carbon.2011.08.039>.
- [12] McCarty RD, Hord J, Roder H. *Selected properties of hydrogen (engineering design data)*. NBS monograph 168. National Bureau of Standards; 1981.
- [13] van den Berg AWC, Areán CO. *Materials for hydrogen storage: current research trends and perspectives*. Chem Commun 2008;668–81. <https://doi.org/10.1039/B712576N>.
- [14] Segakweng T, Musyoka NM, Ren J, et al. *Comparison of MOF-5- and Cr-MOF-derived carbons for hydrogen storage application*. Res Chem Intermed 2016;42:4951–61. <https://doi.org/10.1007/s11164-015-2338-1>.
- [15] Melicchio A, Liguori P, Russo B, Golemme. *Strategy for the enhancement of H2 uptake in porous materials containing TiO2*. Int J Hydrogen Energy 2016;41:5733–40. <https://doi.org/10.1016/j.ijhydene.2016.02.050>.
- [16] Cai J, Li L, Yang C, Zhao X. *Large surface area ordered porous carbons via nanocasting zeolite 10X and high performance for hydrogen storage application*. ACS Appl Mater Interfaces 2014;6:167–75. <https://doi.org/10.1021/am403810j>.
- [17] Dang Y, Guo W, Zhao L, Zhu H. *Porous carbon materials based on graphdiyne basis units by the incorporation of the functional groups and Li atoms for superior CO2 capture and*

- sequestration. *ACS Appl Mater Interfaces* 2017;9. <https://doi.org/10.1021/acsmami.7b10836>. 30002–13.
- [18] Czakkal O, Nagy B, Dobos G, Fouquet P, Bahn E, Laszlo K. Static and dynamic studies of hydrogen adsorption on nanoporous carbon gels. *Int J Hydrogen Energy* 2019;44:18169–78. <https://doi.org/10.1016/j.ijhydene.2019.05.131>.
- [19] Murray LJ, Dincă M, Long JR. Hydrogen storage in metal–organic frameworks. *Chem Soc Rev* 2009;38:1294–314. <https://doi.org/10.1039/b802256a>.
- [20] Firlej L, Roszak Sz, Kuchta B, Pfeifer P, Wexler C. Enhanced hydrogen adsorption in boron substituted carbon nanopores. *J Chem Phys* 2009;131:164702. <https://doi.org/10.1063/1.3251788>.
- [21] Kuchta B, Firlej L, Pfeifer P, Wexler C. Numerical estimation of hydrogen storage limits in carbon-based nanopores. *Carbon* 2010;48:223–31. <https://doi.org/10.1016/j.carbon.2009.09.009>.
- [22] Kuchta B, Firlej L, Roszak S, Pfeifer P. A review of boron enhanced nanoporous carbons for hydrogen adsorption: numerical perspective. *Adsorption* 2010;16:413–21. <https://doi.org/10.1007/s10450-010-9235-0>.
- [23] Kuchta B, Firlej L, Cepel R, Pfeifer P, Wexler C. Structural and energetic factors in designing a nanoporous sorbent for hydrogen storage. *Colloids Surf Physicochem Eng Asp* 2010;357:61–6. <https://doi.org/10.1016/j.colsurfa.2010.01.020>.
- [24] Lachawiec AJ, Qi G, Yang RT. Hydrogen storage in nanostructured carbons by spillover: bridge-building enhancement. *Langmuir* 2005;21:11418–24. <https://doi.org/10.1021/la051659r>.
- [25] Romanos J, Beckner M, Rash T, Firlej L, Kuchta B, Yu P, et al. Nanospace engineering of KOH activated carbon. *Nanotechnology* 2012;23:015401. <https://doi.org/10.1088/0957-4484/23/1/015401>.
- [26] Gogotsi Y, Portet C, Osswald S, Simmons J, Yildirim T, Laudisio G, et al. Importance of pore size in high-pressure hydrogen storage by porous carbons. *Int J Hydrogen Energy* 2009;34:6314–9. <https://doi.org/10.1016/j.ijhydene.2009.05.073>.
- [27] Deng H, Grunder S, Cordova KE, Valente C, Furukawa H, Hmadeh M, et al. Large-pore apertures in a series of metal-organic frameworks. *Science* 2012;336:1018–23. <https://doi.org/10.1126/science.1220131>.
- [28] Tian HY, Buckley CE, Paskevicius M, Sheppard DA, Wang SB, Webb CJ, et al. Nanoscale cobalt doped carbon aerogel: microstructure and isosteric heat of hydrogen adsorption. *Int J Hydrogen Energy* 2011;36:10855–60. <https://doi.org/10.1016/j.ijhydene.2011.06.039>.
- [29] Tian HY, Buckley CE, Sheppard DA, Paskevicius M, Hanna N. A synthesis method for cobalt doped carbon aerogels with high surface area and their hydrogen storage properties. *Int J Hydrogen Energy* 2010;35:13242–6. <https://doi.org/10.1016/j.ijhydene.2010.09.018>.
- [30] Huang J, Liang Y, Dong H, Hu H, Yu P, Peng L, et al. Revealing contribution of pore size to high hydrogen storage capacity. *Int J Hydrogen Energy* 2018;43:18077–82. <https://doi.org/10.1016/j.ijhydene.2018.08.027>.
- [31] Otowa T, Tanibata R, Itoh M. Production and adsorption characteristics of MAXSORB: high-surface area active carbon. *Gas Separ Purif* 1993;7:241–5. [https://doi.org/10.1016/0950-4214\(93\)80024-Q](https://doi.org/10.1016/0950-4214(93)80024-Q).
- [32] Beckner M, Dailly A. Adsorption enthalpy calculations of hydrogen adsorption at ambient temperature and pressures exceeding 300 bar. *Am J Anal Chem* 2013;4:8–16. <https://doi.org/10.4236/ajac.2013.410A3002>.
- [33] Casco ME, Martínez-Escandell M, Gadea-Ramos E, Kaneko K, Silvestre-Albero J, Rodríguez-Reinoso F. High-pressure methane storage in porous materials: are carbon materials in the Pole position? *Chem Mater* 2015;27:959–64. <https://doi.org/10.1021/cm5042524>.
- [34] Rash TA, Gillespie A, Holbrook BP, Hiltzik LH, Romanos J, Soo YC, et al. Microporous carbon monolith synthesis and production for methane storage. *Fuel* 2017;200:371–9. <https://doi.org/10.1016/j.fuel.2017.03.037>.
- [35] Pfeifer P, Suppes G, Shah PS, Burrell J. High surface area carbon and process for its production 2014;8:691. 177 B2.
- [36] Pfeifer P, Suppes G, Shah PS, Burrell J. High surface area carbon and process for its production 2015;8:926. 932 B2.
- [37] Brunauer S, Emmett PH, Teller E. Adsorption of gases in multimolecular layers. *J Am Chem Soc* 1938;60:309–19. <https://doi.org/10.1021/ja01269a023>.
- [38] Neimark A, Ravikovitch P, Lin Y, Thommes M. Quenched solid density functional theory and pore size analysis of micro-mesoporous carbons. *Carbon* 2009;47:1617–28. <https://doi.org/10.1016/j.carbon.2009.01.050>.
- [39] Ravikovitch PI, Neimark AV. Density functional theory model of adsorption on amorphous and microporous silica materials. *Langmuir* 2006;22:11171–9. <https://doi.org/10.1021/la0616146>.
- [40] Thommes M. Physical adsorption characterization of nanoporous materials. *Chem Ing Tech* 2010;82:1059–73. <https://doi.org/10.1002/cite.201000064>.
- [41] Gor G, Thommes M, Cychosz K, Neimark AV. Quenched solid density functional theory method for characterization of mesoporous carbons by nitrogen adsorption. *Carbon* 2012;50:1583–90. <https://doi.org/10.1016/j.carbon.2011.11.037>.
- [42] Zhu Y, Murali S, Stoller M, Ganesh K, Cai W, Ferreira P, et al. Carbon-based supercapacitors produced by activation of graphene. *Science* 2011;332:1537–41. <https://doi.org/10.1126/science.1200770>.
- [43] Romanos J, Beckner M, Stalla D, Tekeci A, Suppes G, Jalilati S, et al. Infrared study of boron–carbon chemical bonds in boron-doped activated carbon. *Carbon* 2013;54:208–14. <https://doi.org/10.1016/j.carbon.2012.11.031>.
- [44] Firlej L, Kuchta B, Lazarewicz A, Pfeifer P. Increased H₂ gravimetric storage capacity in truncated carbon slit pores modeled by Grand Canonical Monte Carlo. *Carbon* 2013;53:208–15. <https://doi.org/10.1016/j.carbon.2012.10.049>.
- [45] Ortiz L, Kuchta B, Firlej L, Roth MW, Wexler C. Methane adsorption in nanoporous carbon: the numerical estimation of optimal storage conditions. *Mater Res Express* 2016;3:055011. <https://doi.org/10.1088/2053-1591/3/5/055011>.
- [46] Michels AMJF, Menon PG, Seldam CA. Adsorption of nitrogen on alumina at high pressure. *Recl Trav Chim Pays-Bas* 1961;80:483–501. <https://doi.org/10.1002/recl.19610800504>.
- [47] Broom DP. The accuracy of hydrogen sorption measurements on potential storage materials. *Int J Hydrogen Energy* 2007;32:4871–88. <https://doi.org/10.1016/j.ijhydene.2007.07.056>.
- [48] Bansal RC, Goyal M. *Activated carbon adsorption*. Boca Raton, FL: Taylor & Francis Group; 2005.
- [49] Otowa T, Nojima Y, Miyazaki T. Development of KOH activated high surface area carbon and its application to drinking water purification. *Carbon* 1997;35:1315–9. [https://doi.org/10.1016/S0008-6223\(97\)00076-6](https://doi.org/10.1016/S0008-6223(97)00076-6).

- [50] Llewellyn P. Characterisation of microporous materials by adsorption microcalorimetry. *Membr Sci Technol* 2007;6:213–30. [https://doi.org/10.1016/S0927-5193\(00\)80010-8](https://doi.org/10.1016/S0927-5193(00)80010-8).
- [51] Myers A, Monson P. Physical adsorption of gases: the case for absolute adsorption as the basis for thermodynamic analysis. *Adsorption* 2014;20:591–622. <https://doi.org/10.1007/s10450-014-9604-1>.
- [52] Burress J, Bethea D, Troub B. Combination volumetric and gravimetric sorption instrument for high accuracy measurements of methane adsorption. *Rev Sci Instrum* 2017;88:053902. <https://doi.org/10.1063/1.4982889>.
- [53] Aranovich G, Donohue M. Determining surface areas from linear adsorption isotherms at supercritical conditions. *J Colloid Interface Sci* 1997;194:392–7. <https://doi.org/10.1006/jcis.1997.5099>.
- [54] Saha D, Wei Z, Deng S. Equilibrium, kinetics and enthalpy of hydrogen adsorption in MOF-177. *Int J Hydrogen Energy* 2008;33:7479–88. <https://doi.org/10.1016/j.ijhydene.2008.09.053>.
- [55] Stadie NP, Murialdo M, Ahn CC, Fultz B. Anomalous isosteric enthalpy of adsorption of methane on zeolite-templated carbon. *J Am Chem Soc* 2013;135:990–3. <https://doi.org/10.1021/ja311415m>.
- [56] Poirier E, Dailly A. Thermodynamics of hydrogen adsorption in MOF-177 at low temperatures: measurements and modelling. *Nanotechnology* 2009;20. <https://doi.org/10.1088/0957-4484/20/20/204006>.
- [57] Donohue M, Aranovich G. Classifications of gibbs adsorption isotherms. *Adv Colloid Interface Sci* 1998;76–77:137–52. [https://doi.org/10.1016/S0001-8686\(98\)00044-X](https://doi.org/10.1016/S0001-8686(98)00044-X).
- [58] Bénard P, Chahine R. Modeling of high-pressure adsorption isotherms above the critical temperature on microporous adsorbents: application to methane. *Langmuir* 1997;13:808–13. <https://doi.org/10.1021/la960843x>.
- [59] Beckner M. *Hydrogen adsorption studies of engineered and chemically modified activated carbons*. University of Missouri–Columbia; 2012.
- [60] Poirier E, Dailly A. Investigation of the hydrogen state in IRMOF-1 from measurements and modeling of adsorption isotherms at high gas densities. *J Phys Chem C* 2008;112:13047–52. <https://doi.org/10.1021/jp800981f>.
- [61] Redlich O, Peterson DL. A useful adsorption isotherm. *J Phys Chem* 1959;63. <https://doi.org/10.1021/j150576a611>. 1024–1024.
- [62] BS EN. Natural stone test methods. Determination of real density and apparent density and of total and open porosity. 2006.
- [63] Prosniewski MJ, Rash TA, Knight EW, Gillespie AK, Stalla D, Schulz CJ, et al. Controlled charge and discharge of a 40-L monolithic adsorbed natural gas tank. *Adsorption* 2018;24:541–50. <https://doi.org/10.1007/s10450-018-9961-2>.
- [64] Pfeifer P, Little R, Rash T, Romanos J, Maland B. *Advanced natural gas fuel tank project*. Sacramento: California Energy Commission; 2016.
- [65] Pfeifer P, Wexler C, Suppes G, Hawthorne F, Jalisatgi S, Lee M, et al. Multiply surface-functionalized nanoporous carbon for vehicular hydrogen storage. 2011.
- [66] Pfeifer P, Gillespie AK, Stalla D, Dohnke E. Multiply surface-functionalized nanoporous carbon for vehicular hydrogen storage—final technical report. Washington, DC: U.S. Department of Energy; 2017.
- [67] Rash T. *A comprehensive report on preparing and analyzing adsorptive materials suitable for hydrogen and methane storage*. University of Missouri–Columbia; 2014.
- [68] Dohnke E. *On the high density hydrogen films adsorbed in carbon nanopores*. University of Missouri–Columbia; 2015.
- [69] Gillespie A. *Properties of adsorbed hydrogen and methane films on nanoporous solids*. University of Missouri–Columbia; 2017.
- [70] Prosniewski M, Gillespie A, Knight E, Rash T, Stalla D, Romanos J, et al. Evaluating methane adsorbed film densities on activated carbon in dynamic systems. *J Energy Storage* 2018;20:357–63. <https://doi.org/10.1016/j.est.2018.10.017>.
- [71] Olsen RJ, Firlej L, Kuchta B, Taub H, Pfeifer P, Wexler C. Sub-nanometer characterization of activated carbon by inelastic neutron scattering. *Carbon* 2011;49:1663–71. <https://doi.org/10.1016/j.carbon.2010.12.051>.
- [72] Olsen RJ, Beckner M, Stone MB, Pfeifer P, Wexler C, Taub H. Quantum excitation spectrum of hydrogen adsorbed in nanoporous carbons observed by inelastic neutron scattering. *Carbon* 2013;58:46–58. <https://doi.org/10.1016/j.carbon.2013.02.026>.